

HIGH ORDER CARTESIAN METHOD FOR THE SHALLOW WATER EQUATIONS ON A SPHERE

November 7, 2001

Prepared by

John B. Drake

William Putman

Paul N. Swarztrauber

David L. Williamson

DOCUMENT AVAILABILITY

Reports produced after January 1, 1996, are generally available free via the U.S. Department of Energy (DOE) Information Bridge:

Web Site: <http://www.osti.gov/bridge>

Reports produced before January 1, 1996, may be purchased by members of the public from the following source:

National Technical Information Service
5285 Port Royal Road
Springfield, VA 22161
Telephone: 703-605-6000 (1-800-553-6847)
TDD: 703-487-4639
Fax: 703-605-6900
E-mail: info@ntis.fedworld.gov
Web site: <http://www.ntis.gov/support/ordernowabout.htm>

Reports are available to DOE employees, DOE contractors, Energy Technology Data Exchange (ETDE), and International Nuclear Information System (INIS) representatives from the following sources:

Office of Scientific and Technical Information
P.O. Box 62
Oak Ridge, TN 37831
Telephone: 865-576-8401
Fax: 865-576-5728
E-mail: reports@adonis.osti.gov
Web site: <http://www.osti.gov/contact.html>

This report was prepared as an account of work sponsored by an agency of the United States Government. Neither the United States nor any agency thereof, nor any of their employees, makes any warranty, express or implied, or assumes any legal liability or responsibility for the accuracy, completeness, or usefulness of any information, apparatus, product, or process disclosed, or represents that its use would not infringe privately owned rights. Reference herein to any specific commercial product, process, or service by trade name, trademark, manufacturer, or otherwise, does not necessarily constitute or imply its endorsement, recommendation, or favoring by the United States Government or any agency thereof. The views and opinions of authors expressed herein do not necessarily state or reflect those of the United States Government or any agency thereof.

HIGH ORDER CARTESIAN METHOD FOR THE SHALLOW WATER EQUATIONS ON A SPHERE

John B. Drake
Computer Science and Mathematics Division
Oak Ridge National Laboratory
William Putman

NASA Goddard Space Flight Center
Greenbelt, MD
Paul N. Swarztrauber

Scientific Computing Division
National Center for Atmospheric Research
Boulder, CO
David L. Williamson

Global Climate Division
National Center for Atmospheric Research
Boulder, CO

Date Published: November 7, 2001

Prepared by
OAK RIDGE NATIONAL LABORATORY
Oak Ridge, Tennessee 37831-6285
managed by
UT-Battelle, LLC
for the
U.S. DEPARTMENT OF ENERGY
under contract DE-AC05-00OR22725

Contents

| | |
|--|-----------|
| LIST OF FIGURES | iv |
| ACKNOWLEDGMENTS | v |
| ABSTRACT | vi |
| 1 INTRODUCTION | 1 |
| 2 THE SHALLOW WATER EQUATIONS ON A SPHERE | 3 |
| 3 LOCAL CARTESIAN SPECTRAL APPROXIMATION | 7 |
| 3.1 NUMERICAL RESULTS FOR THE GRADIENT APPROXIMATION | 9 |
| 3.2 SYMMETRIC TIME INTEGRATION METHOD | 11 |
| 4 TEST CASES | 13 |
| 4.1 STEADY, ZONAL FLOW TEST | 13 |
| 4.2 ZONAL FLOW OVER AN ISOLATED MOUNTAIN | 15 |
| 4.3 ANALYZED 500mb INITIAL CONDITIONS | 21 |
| 5 CONCLUSIONS | 29 |

List of Figures

| | | |
|----|---|----|
| 1 | Approximation stencil for a regular point of an icosahedral grid. | 10 |
| 2 | Convergence of the Gradient Approximations. Curves for a) npts=7, N=9; b) npts=13, N=16; c) npts=19, N=25 | 11 |
| 3 | Relative RMS Error in velocity, Test Case 2, $q = 2, 3, 4$. Standard Form | 13 |
| 4 | Relative RMS Error in height, Test Case 2, $q = 2, 3, 4$. Standard Form | 14 |
| 5 | Relative RMS Error in Velocity, Test Case 2, $q = 2, 3, 4$. Rotational Form | 14 |
| 6 | Relative RMS Error in Height, Test Case 2, $q = 2, 3, 4$. Rotational Form | 15 |
| 7 | Conserved integral quantities. Test Case 5, $q = 4$. Rotational Form | 16 |
| 8 | Initial condition wave, Test Case 5, 6th order at 6 hrs | 17 |
| 9 | Initial wave, Test Case 5, 6th order at 18 hrs | 18 |
| 10 | Focused grid, 2nd order at 15 days | 19 |
| 11 | Uniform grid, 5th order at 15 days | 20 |
| 12 | Conserved integral quantities. Test Case 7a, $q = 5$ | 21 |
| 13 | Reference Solution at 5 Days | 22 |
| 14 | Cartesian Solution at day 5, Fifth order, uniform ($q = 5$)-grid | 23 |
| 15 | Instability of overdetermined, focused approximation, ($q = 4$)-grid | 24 |
| 16 | Underdetermined, focused approximation, ($q = 4$)-grid | 25 |
| 17 | Focused approximation, Fifth order, ($q = 4$)-grid | 26 |
| 18 | Global Mean Absolute Error Comparison | 27 |
| 19 | Northern Hemisphere Mean Absolute Error Comparison | 28 |

ACKNOWLEDGEMENTS

This research was supported by the Climate Change Prediction Program of the Atmospheric and Climate Research Division, Office of Energy Research, U.S. Department of Energy under contract DE-AC05-00OR22725 with UT-Battelle, LLC and by the National Science Foundation supporting research of the National Center for Atmospheric Research. Computing resources were provided by the Center for Computational Science – Climate and Carbon Research at Oak Ridge National Laboratory.

ABSTRACT

The shallow water equations in a spherical geometry are solved using a 3-dimensional Cartesian method. Spatial discretization of the 2-dimensional, horizontal differential operators is based on the Cartesian trivariate polynomial form of the spherical harmonics and an icosahedral (spherical) grid. Second thru fifth order methods are obtained by inclusion of the appropriate spherical harmonics. A family of symmetric time integration schemes indexed by the parameter β which includes the explicit leapfrog, the implicit Simpson's and trapezoidal rules are investigated in conjunction with the spatial discretizations. Reasonable stability properties and the ability to perform long integrations of the nonlinear equations are documented for the implicit methods. Error measures and conservation properties of the method are reported for flow over a mountain and a real data case from a test suite for shallow water equation models.

1 INTRODUCTION

Several early papers investigated the use of icosahedral- triangular meshes [13, 14, 22, 23, 24, 25]. The barotropic vorticity equation and the shallow water equations on the sphere served as the primary equation sets for testing the numerical methods because of their relevance in atmospheric flow models. A review article [26] gives further references of early work.

More recently icosahedral meshes have been used with a method based on the stream function and velocity potential formulation of the shallow water equations with a control volume discretization [11]. The method was refined and tested on a standard set of cases [27] by Heikes and Randall in [7, 8]. Other icosahedral methods have also been proposed in [1].

The Cartesian form of the shallow water equations was proposed by Swarztrauber in [27] and further developed in [20]. This alternative formulation avoids the singularity in the velocity at the pole by expressing velocities in a 3-D Cartesian form instead of in spherical coordinates. The introduction of 3-D velocities necessitates a change of the form of the shallow water equations. At first sight this form appears more complicated and probably more expensive computationally. But a closer examination shows the Cartesian formulation to be compact and computationally simple.

The Cartesian geometry of the sphere and the discretization of the sphere using the points of an icosahedral triangular mesh lead to a computational economy at the poles. The distances between points of this mesh are nearly uniform and thus there is not a CFL restriction on timestep arising from a longitudinal concentration of points near the pole. There is no need to filter the solution near the poles, a step that can be costly for some methods and that introduces errors on all scales.

The Cartesian formulation was used with the calculation of derivatives using a spectral vector harmonic method in [19]. In this paper we consider the Cartesian formulation with a local calculation of derivatives using a stencil of points located on an icosahedral grid. The derivative approximations might be characterized as locally spectral in that they are based on spherical harmonics but only use a local stencil of points, essentially a finite difference method. We show by numerical experiments that the method of approximating differential operators on the icosahedral mesh is accurate and converges as the mesh is refined. Thus the discretizations are consistent with the PDE's.

Since the number of points of the stencil and the number of spherical harmonics used in the derivation of the difference formulae are somewhat arbitrary, high order methods are easily

obtained. An earlier paper studied the performance of this method for a second order approximation. Here we study stencils with up to 43 points and approximations up to 6th order. Stability of the higher order methods is a major issue and is partially addressed with the use of implicit time integration schemes. A family of symmetric time integration methods is used. The family includes the explicit leapfrog, trapezoidal rule and Simpson's methods.

The discretization is then applied to the shallow water equations on a sphere and tested on two cases of a set of standard cases for shallow water equation solvers. These tests highlight many of the positive properties of the method as well as expose some of its short comings. We pay particular attention to the stability and accuracy properties of the method.

2 THE SHALLOW WATER EQUATIONS ON A SPHERE

The momentum and mass continuity equations for shallow water flows can be written in advective form

$$\frac{d\mathbf{v}}{dt} = -f\mathbf{k} \times \mathbf{v} - g\nabla h + \mathbf{F}_v, \quad (1)$$

and

$$\frac{dh^*}{dt} = -h^*\nabla \cdot \mathbf{v} + F_h \quad (2)$$

where the substantial derivative is given by

$$\frac{d}{dt}(\cdot) \equiv \frac{\partial}{\partial t}(\cdot) + \mathbf{v} \cdot \nabla(\cdot). \quad (3)$$

The velocity is referred to a rotating Cartesian frame and the components of $\mathbf{v} = (u, v)$ are in the longitudinal and latitudinal directions respectively. The height of the free surface is defined $h = h^* + h_s$ where h^* is the depth of the fluid and the bottom surface height is given by the time invariant function h_s . External forcing, if present, is included in $\mathbf{F}_v = (F_u, F_v)$ and F_h . This form of the equation is not in conservative form and consequently the numerical methods we develop will not be strictly conservative.

It may be advantageous to evaluate the horizontal (surface) derivatives using a Cartesian form. This form was developed in detail in [20]. By extending the surface vector $\mathbf{v} = (u, v)^T$ to the three-dimensional $\mathbf{v}_s = (w, v, u)^T$ the shallow water equations can be embedded in the system

$$\frac{\partial \mathbf{v}_s}{\partial t} + \mathbf{S}(\mathbf{v}_s)\mathbf{v}_s + \boldsymbol{\alpha} + \boldsymbol{\beta} + \boldsymbol{\gamma} + \boldsymbol{\delta} = 0, \quad (4)$$

where

$$\mathbf{S}(\mathbf{v}_s) = \begin{pmatrix} \frac{\partial w}{\partial r} & \frac{1}{a}(\frac{\partial w}{\partial \theta} - v) & \frac{1}{a \cos \theta}(\frac{\partial w}{\partial \lambda} - u \cos \theta) \\ \frac{\partial v}{\partial r} & \frac{1}{a}(\frac{\partial v}{\partial \theta} + w) & \frac{1}{a \cos \theta}(\frac{\partial v}{\partial \lambda} - u \sin \theta) \\ \frac{\partial u}{\partial r} & \frac{1}{a} \frac{\partial u}{\partial \theta} & \frac{1}{a \cos \theta}(\frac{\partial u}{\partial \lambda} - v \sin \theta + w \cos \theta) \end{pmatrix}, \quad (5)$$

r is the radial coordinate ($r = a$ at the earth's surface) and

$$\boldsymbol{\alpha} = \begin{pmatrix} \frac{u^2 + v^2}{a} \\ 0 \\ 0 \end{pmatrix}, \quad (6)$$

$$\boldsymbol{\beta} = \begin{pmatrix} 0 \\ \frac{g}{a} \frac{\partial h}{\partial \theta} \\ \frac{g}{a \cos \theta} \frac{\partial h}{\partial \lambda} \end{pmatrix}, \quad (7)$$

$$\boldsymbol{\gamma} = \begin{pmatrix} 0 \\ -F_v \\ -F_u \end{pmatrix}, \quad (8)$$

and

$$\boldsymbol{\delta} = \begin{pmatrix} 0 \\ fu \\ -fv \end{pmatrix}. \quad (9)$$

If we define $\mathbf{V} = (X, Y, Z)^T$ as the velocity in Cartesian coordinates (x, y, z) then

$$\mathbf{v}_s = \mathbf{Q}\mathbf{V} \quad (10)$$

where

$$\mathbf{Q} = \begin{pmatrix} \cos \theta \cos \lambda & \cos \theta \sin \lambda & \sin \theta \\ -\sin \theta \cos \lambda & -\sin \theta \sin \lambda & \cos \theta \\ -\sin \lambda & \cos \lambda & 0 \end{pmatrix}. \quad (11)$$

Substituting (62) into (57) and multiplying by \mathbf{Q}^T we obtain the Cartesian form

$$\frac{\partial \mathbf{V}}{\partial t} + \mathbf{C}\mathbf{V} + \mathbf{Q}^T(\boldsymbol{\alpha} + \boldsymbol{\beta} + \boldsymbol{\gamma} + \boldsymbol{\delta}) = 0. \quad (12)$$

In this equation

$$\mathbf{C} = \mathbf{Q}^T \mathbf{S} \mathbf{Q} = \begin{pmatrix} \frac{\partial X}{\partial x} & \frac{\partial X}{\partial y} & \frac{\partial X}{\partial z} \\ \frac{\partial Y}{\partial x} & \frac{\partial Y}{\partial y} & \frac{\partial Y}{\partial z} \\ \frac{\partial Z}{\partial x} & \frac{\partial Z}{\partial y} & \frac{\partial Z}{\partial z} \end{pmatrix}, \quad (13)$$

$$\mathbf{Q}^T \boldsymbol{\alpha} = \frac{1}{a^2} \begin{pmatrix} x(X^2 + Y^2 + Z^2) \\ y(X^2 + Y^2 + Z^2) \\ z(X^2 + Y^2 + Z^2) \end{pmatrix}, \quad (14)$$

$$\mathbf{Q}^T \boldsymbol{\delta} = \frac{2\Omega z}{a^2} \begin{pmatrix} 0 & -z & y \\ z & 0 & -x \\ -y & x & 0 \end{pmatrix} \begin{pmatrix} X \\ Y \\ Z \end{pmatrix}, \quad (15)$$

and

$$\mathbf{Q}^T \boldsymbol{\beta} = g\mathbf{P}\nabla_c h \quad (16)$$

where

$$\mathbf{P} = \frac{1}{a^2} \begin{pmatrix} a^2 - x^2 & -xy & -xz \\ -xy & a^2 - y^2 & -yz \\ -xz & -yz & a^2 - z^2 \end{pmatrix}, \quad (17)$$

and

$$\nabla_c h = \left(\frac{\partial h}{\partial x}, \frac{\partial h}{\partial y}, \frac{\partial h}{\partial z} \right)^T. \quad (18)$$

Similarly the continuity equation in Cartesian form is

$$\frac{\partial h^*}{\partial t} + \mathbf{V}^T \mathbf{P} \nabla_c h^* + h^* \nabla_c \cdot \mathbf{V} = F_h. \quad (19)$$

The matrix P projects an arbitrary Cartesian vector onto a plane that is tangent to the sphere at the point (x, y, z) .

Another form of the momentum equation can be developed around the vorticity and the kinetic energy. The vorticity ζ is defined in the spherical coordinate system as $\zeta \equiv \mathbf{k} \cdot \nabla \times \mathbf{v}$. Using the vector identity

$$\mathbf{v} \cdot \nabla \mathbf{v} = \nabla \left(\frac{\mathbf{v} \cdot \mathbf{v}}{2} \right) + \zeta \mathbf{k} \times \mathbf{v}, \quad (20)$$

the momentum equation can be written

$$\frac{\partial \mathbf{v}}{\partial t} = -(\zeta + f) \mathbf{k} \times \mathbf{v} - \nabla \left(gh + \frac{\mathbf{v} \cdot \mathbf{v}}{2} \right) + \mathbf{F}_v. \quad (21)$$

Changing variables to Cartesian velocities the resulting Cartesian equation is

$$\frac{\partial \mathbf{V}}{\partial t} + \mathbf{Q}^T (\boldsymbol{\Lambda} + \boldsymbol{\gamma} + \boldsymbol{\Delta}) = 0. \quad (22)$$

In this equation

$$\mathbf{Q}^T \boldsymbol{\Delta} = \frac{(\zeta + 2\Omega z)}{a^2} \begin{pmatrix} 0 & -z & y \\ z & 0 & -x \\ -y & x & 0 \end{pmatrix} \begin{pmatrix} X \\ Y \\ Z \end{pmatrix}, \quad (23)$$

and

$$\mathbf{Q}^T \mathbf{\Lambda} = \mathbf{P} \nabla_c (gh + \frac{\mathbf{V} \cdot \mathbf{V}}{2}). \quad (24)$$

Since the *curl* is invariant under coordinate transformation we have that $\zeta \equiv \mathbf{k} \cdot \nabla_c \times \mathbf{V}$ where \mathbf{k} is the unit vector in the direction normal to the sphere at the point (x, y, z) . That is, $\mathbf{k} = \frac{\mathbf{x}}{a}$. (This notation in Cartesian coordinates should not be confused with the standard notation \mathbf{k} for the unit vector in the z -direction.) The Cartesian *curl* is the standard,

$$\nabla_c \times \mathbf{V} = \begin{pmatrix} \frac{\partial Z}{\partial y} - \frac{\partial Y}{\partial z} \\ \frac{\partial X}{\partial z} - \frac{\partial Z}{\partial x} \\ \frac{\partial Y}{\partial x} - \frac{\partial X}{\partial y} \end{pmatrix}. \quad (25)$$

These derivatives are available from the \mathbf{C} matrix described above.

3 LOCAL CARTESIAN SPECTRAL APPROXIMATION

The spherical harmonic functions form a basis for functions defined on the surface of the sphere. They have long been used in climate and weather models as the basis for the spectral method [10] and for the approximation of derivatives on the surface of the sphere [18]. The spherical harmonic, Y_n^m can be defined with the normalized associated Legendre functions $P_n^m(\theta)$ by

$$Y_n^m(\lambda, \theta) = e^{im\lambda} \bar{P}_n^m(\theta). \quad (26)$$

The normalized associated Legendre polynomials can be defined from Rodrigues' formula [17]

$$\bar{P}_n^m(\theta) = (-1)^m \left[\frac{2n+1}{2} \frac{(n-m)!}{(n+m)!} \right]^{1/2} \frac{1}{2^n n!} (\sin \theta)^m \frac{d^{m+n}}{dz^{m+n}} (z^2 - 1)^n \quad (27)$$

where $z = \cos \theta$ and θ is colatitude. (In this section only θ refers to colatitude while in other sections it refers to latitude.) Equations (26) and (27) are combined to give a formula for the Cartesian representation of the spherical harmonics [21].

$$Y_n^m(x, y, z) = C_n^m (x + iy)^m \frac{d^{m+n}}{dz^{m+n}} (z^2 - 1)^n, \quad (28)$$

where

$$C_n^m = \frac{(-1)^m}{2^n n!} \left[\frac{2n+1}{2} \frac{(n-m)!}{(n+m)!} \right]^{1/2}. \quad (29)$$

Any linear operator L on functions on a sphere can be approximated directly by requiring that the discrete operator act correctly on the selected basis functions. Given a cluster of points $\{p_l\}$, $l = 0, \dots, npts - 1$ on the surface of the sphere and a tabulation of a function U , $\{U(p_l)\}$ about the point p_0 , we wish to determine coefficients c_l such that

$$L(U)(p_0) \approx \sum_{l=0}^{npts-1} c_l U(p_l). \quad (30)$$

(The sense of the approximation (\approx) must be described.) We require (30) to hold locally at p_0 for all spherical harmonics through some number N ,

$$L(r^n Y_n^m)(p_0) \cong \sum_{l=0}^{npts-1} c_l r^n Y_n^m(p_l). \quad (31)$$

The spherical harmonics Y_n^m are ordered so that with increasing number the degree increases,

Equation (31) is solved for the c_i at each point p_0 . Thus a local spectral approximation is obtained in the form of coefficients for a stencil of neighboring points. This approach is general and is applicable to any distribution of points on the sphere.

The sense of the approximation in (30) is as a least squares problem for (31). The problem can be stated in matrix form: find \mathbf{c} which minimizes

$$\|\mathbf{H}\mathbf{c} - \mathbf{d}\|_2^2 \tag{32}$$

where \mathbf{H} is a $N \times npts$ matrix of spherical harmonics evaluated at points of the stencil and \mathbf{d} is the vector of the exact linear operator applied to the harmonics evaluated at the point. The least squares problem can be solved elegantly using the singular value decomposition (SVD) [9]. Let $\mathbf{H} = \mathbf{U}\mathbf{S}\mathbf{V}^T$ be the SVD. The matrix $\mathbf{S} = \text{diag}(\sigma_1, \sigma_2, \dots, \sigma_{npts})$ is the matrix of singular values in descending order. The solution to the least squares problem is

$$\mathbf{c} = \mathbf{V}\mathbf{S}^{-1}\mathbf{U}^T\mathbf{d} \tag{33}$$

The choice of N and $npts$ determine the formal accuracy and smoothness of the derivative approximations. In general, we choose $npts$ points nearly symmetric about the point p_0 . The number of points used in the stencil will determine the efficiency of the method because evaluation of the derivatives requires a combination of values from these neighboring points. For the icosahedral grid, each point has 5 or 6 immediate neighbors ($npts = 7$). (See Figure 1.) If all the immediate neighbors of each of these are included in the stencil, then $npts = 19$. If only neighbors common to two of the immediate neighbors are included (the six pointed star), then a stencil with $npts = 13$ results. For higher order methods, we allow inclusion of immediate, secondary or tertiary neighbors. Up to $npts = 43$ is admissible. These neighbors are identified using the icosahedral grid structure. This is the only function, however, for the grid. Otherwise, the method might be considered meshless.

A smoothing parameter that can be introduced in the approximation is the truncation level in the SVD solution. The diagonal matrix of singular values, \mathbf{S} , can be used to smooth the least squares solution when the system is underdetermined. By truncating the singular values that are smaller than some tolerance, the minimum norm solution for \mathbf{c} is obtained. This truncation gives a solution regardless of the underdetermined or overdetermined nature of the least squares problem. We have found it advantageous to use the same truncation at all points. For $npts = 7$, we truncate at six because the primary points of the icosahedron have only five neighbors. The

coefficients are unique at these points and of minimum norm at the other points.

For the shallow water equations, the stencil coefficients are calculated for each of the linear operators $L(U) = \frac{\partial U}{\partial x}, \frac{\partial U}{\partial y}, \frac{\partial U}{\partial z}$, and the Laplacian, ΔU . The derivative approximations when combined form the gradient operator. Since the gradient of a function defined only on the sphere is always tangent to the sphere, the approximation is projected onto the sphere.

The Laplacian is used to introduce artificial diffusion in order to enhance the stability of the time integration. The discretization of the Laplacian follows the same approach as the approximation of the derivative operators. Thus, it is not based on repeated application of the derivatives.

The accuracy of the method is determined by the formal order of accuracy and the smoothing properties of the least squares solution. We use the first 49 spherical harmonics to produce a formally 6th order method. But depending on the choice of the number of points in the stencil, the least squares problem is overdetermined or underdetermined. Numerical experimentation has lead us to the choice of the parameters.

3.1 NUMERICAL RESULTS FOR THE GRADIENT APPROXIMATION

The basic icosahedral mesh consists of twenty triangles on 12 grid points. Each of the twelve points of the mesh is connected to five neighboring points. The refinements of this mesh are subdivisions of the twenty base triangles. By placing three points on the edges of each large triangle, one on each side and dividing each triangle into three subtriangles, the $q = 0$ mesh is obtained by projection of the points (and edges) onto the surface of the sphere. Halving this mesh results in the $q = 1$ mesh and again halving gives the $q = 2$ mesh. The number of points in the mesh is given by the formula,

$$GP(q) = 5(2^{2q+3}) + 2 \tag{34}$$

Table 1 gives geometric information about the different icosahedral meshes.

To check the accuracy of the gradient approximations, a test function exhibiting all modes was used,

$$\phi(x, y, z) = a(\exp x + \exp y + \exp z) \tag{35}$$

The errors in the following tables are derived from the Cartesian approximation to the gradient of this function. The exact values of the function at the vertices of the icosahedral mesh are computed and used in the difference formulas to approximate the Cartesian derivatives. The

| q | Grid Points | Triangles | h_{min} (km) | h_{max} (km) | h_{ave} (km) | h_{min}/h_{max} |
|---|-------------|-----------|----------------|----------------|----------------|-------------------|
| - | 12 | 20 | 6699.0 | 6699.0 | 6699.0 | 1.0000 |
| 0 | 42 | 80 | 3482.0 | 3938.0 | 3710.0 | 0.8843 |
| 1 | 162 | 320 | 1613.0 | 2070.0 | 1901.0 | 0.7792 |
| 2 | 642 | 1280 | 761.1 | 1049.0 | 956.2 | 0.7255 |
| 3 | 2562 | 5120 | 368.4 | 526.3 | 478.8 | 0.7001 |
| 4 | 10242 | 20480 | 181.2 | 263.4 | 239.5 | 0.6878 |
| 5 | 40962 | 20480 | 89.8 | 131.7 | 119.8 | 0.6818 |

Table 1: Geometric information for icosahedral grids

Cartesian gradient is then transformed to spherical coordinates and compared with the exact gradient of ϕ . The error reported is the l^2 -error over the points of the icosahedral mesh.

The number of spherical harmonics used will determine the order of the approximation. If $N = 9$, then spherical harmonics of second order are used. If $N = 16$, then third order harmonics are included. For $N = 25$, fourth order harmonics are included. These clusters define the stencil (see Figure 1) of the discrete operator.

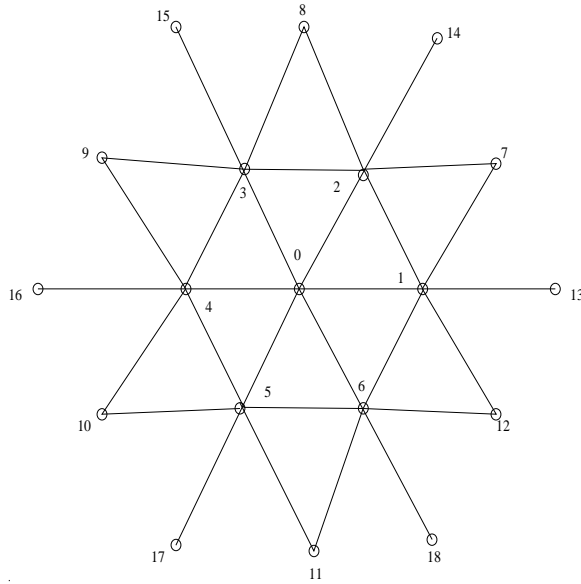


Fig. 1: Approximation stencil for a regular point of an icosahedral grid.

Figure 2 is a plot of the gradient approximation error with a log-log scale. It shows the convergence of the gradient approximation as the mesh size is decreased. The rate of convergence is estimated from the amount of decrease in the error as the mesh size is halved. If the error is proportional to h^p , then by halving the mesh size the error will reduce by a factor of 2^p . Using a stencil of seven points ($npts = 7$) and the harmonics through second order ($N = 9$) yields second

order convergence ($p = 2.0$). With a stencil of 13 points and harmonics through third order we get somewhat better than third order convergence. Fourth order convergence is obtained using a nineteen point stencil and twenty five harmonics.

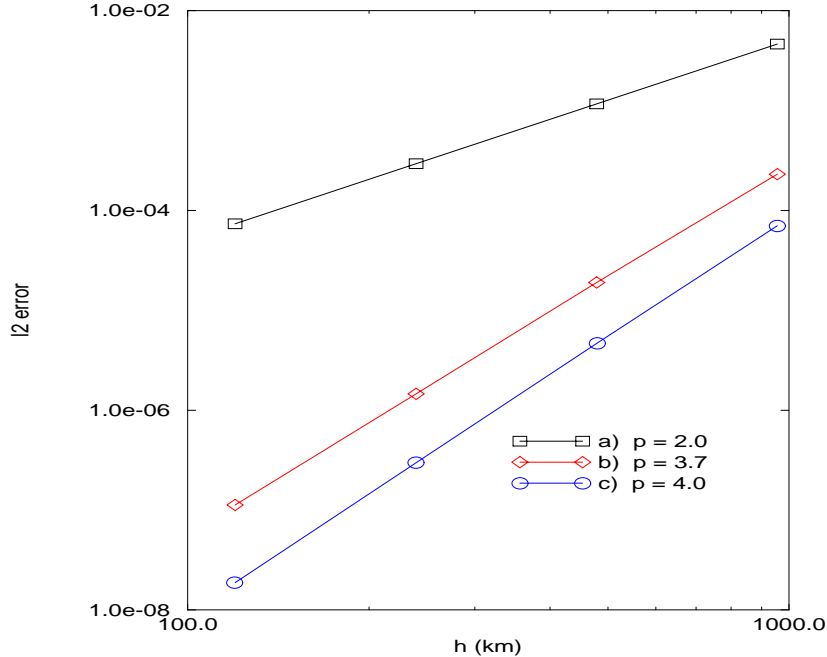


Fig. 2: Convergence of the Gradient Approximations. Curves for a) $npts=7$, $N=9$; b) $npts=13$, $N=16$; c) $npts=19$, $N=25$

The precision of the singular value computation becomes an issue for the higher order methods at resolutions above $q = 4$. By computing the stencil coefficients in extended precision consistent results were obtained. A similar situation holds with regards to the computation of Gaussian quadrature points for high resolution spectral methods. Since these calculations can be performed once for each grid the computational cost is not of great concern.

The discretization method can be applied to other grids as well. A grid with variable resolution, focusing a high resolution grid over an area of interest, has shown promise in several studies [4, 2, 3, 28]. A Schmidt [16] transformation of the uniform grid using a stretching factor of $c = 2$ was used to generate focused grids for the terrain case and the real data case. The stretch factor of two implies a doubling of the distance between grid points away from the focused area, but a halving of the mesh distances near the focused point.

3.2 SYMMETRIC TIME INTEGRATION METHOD

The explicit mid-point time integration scheme is commonly used for the integration of the shallow water equations. Sanz-Serna [15] has shown why this rule is advantageous for the

integration of Hamiltonian systems and analyzed the nonlinear stability properties. The property of symmetry defined by the ability to integrate either forward in time or backward in time, is key. Here we use the family of symmetric ODE integration methods studied in [6] that includes the explicit mid-point rule as well as the symmetric implicit trapezoidal rule.

The family solves the ODE $y' = f(t, y)$. It is indexed with a continuous free parameter β and is defined by

$$y^{n+1} = y^{n-1} + \Delta t[\beta f^{n+1} + 2(1 - \beta)f^n + \beta f^{n-1}]. \quad (36)$$

If $\beta = 0$, then the explicit leapfrog (mid-point) rule results. If $\beta = 1$, then the implicit trapezoidal rule results. If $\beta = \frac{1}{3}$ then the third order error terms of the midpoint and trapezoidal rules cancel leaving Simpson's rule, which has a fifth order error term.

Analysis of this method [5] for integration of weakly stable limit cycle problems, suggests that a value of $\beta > \frac{2}{3}$ yields proper dynamical behavior. We have used the value $\beta = 0.7$ in this study.

The update is organized as an explicit predictor followed by a corrector. The explicit predictor is the mid-point rule.

$$y^* = y^{n-1} + 2\Delta t f^n, \quad (37)$$

$$b^n = y^* + \Delta t[-2\beta f^n + \beta f^{n-1}]. \quad (38)$$

Then an iteration starting with $k = 0, 1, \dots$, is performed to solve the remaining implicit equation

$$y^{k+1} = b^n + \Delta t \beta f(y^k). \quad (39)$$

The starting value of the iteration is $y^0 = y^*$.

4 TEST CASES

A set of test cases for the shallow water equations on a sphere are detailed in [27]. These cases provide a rigorous test of methods as well as allowing for comparison between methods.

4.1 STEADY, ZONAL FLOW TEST

Test case 2 is a steady, non-linear zonal flow rotated through an angle $\alpha = \frac{\pi}{4}$. It tests the ability of the code to maintain a steady state solution independent of the grid orientation and gives a good idea of the accuracy of the methods. The velocity and geopotential for this test case are exactly representable with the spherical harmonics of second order. So the local spherical harmonic approximations for the derivative operators are able to capture the steady state solution extremely well. Figure 3 and 4 show the error, as a function of time, in the velocity (using the relative RMS error with the exact steady solution) and the RMS error in the height field, respectively. The $q = 2, 3$ integrations used a time step of 1200 seconds for the 5 day (120 hour) simulations while the $q = 4$ mesh used a 600 second timestep.

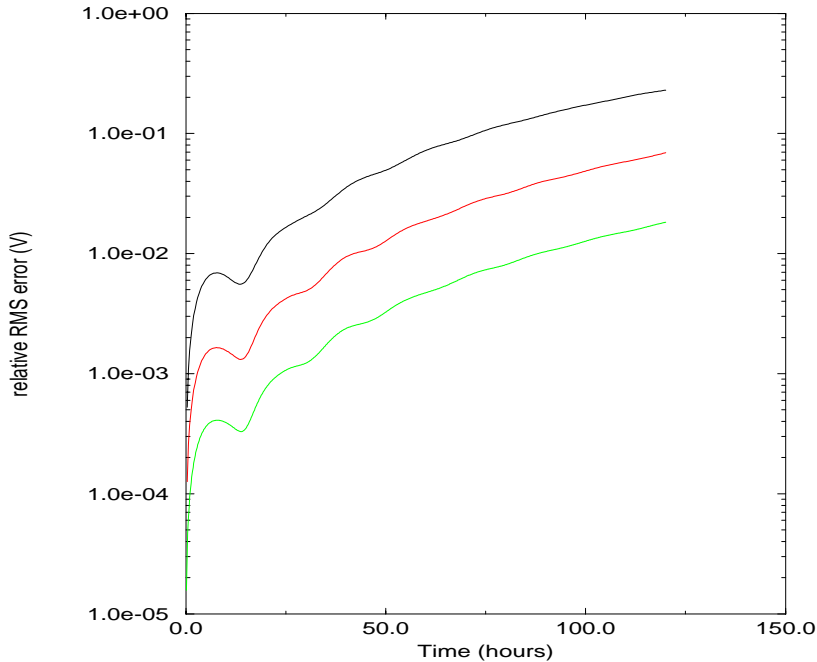


Fig. 3: Relative RMS Error in velocity, Test Case 2, $q = 2, 3, 4$. Standard Form

Figure 5 and 6 show the velocity error and the height error for the Cartesian equations also using the quadratic approximation on 6 or 7 neighbors. The error growth is much more controlled.

The third order method on 13 points without filtering for test case 2 gives errors as shown

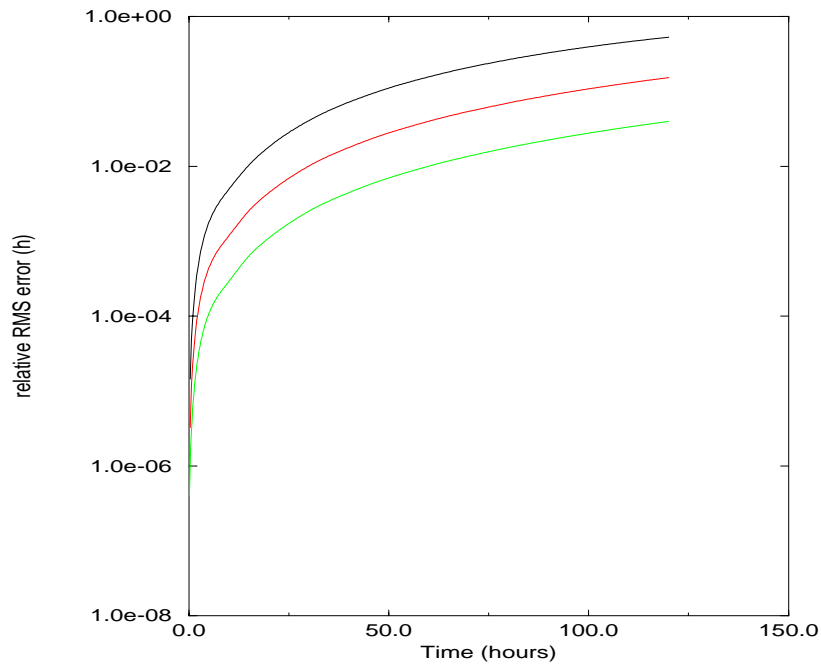


Fig. 4: Relative RMS Error in height, Test Case 2, $q = 2, 3, 4$. Standard Form

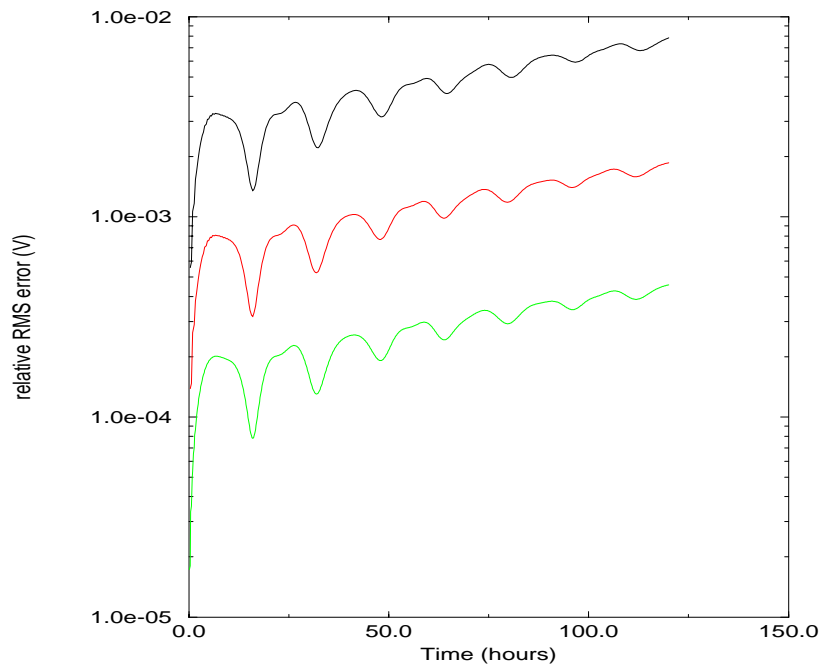


Fig. 5: Relative RMS Error in Velocity, Test Case 2, $q = 2, 3, 4$. Rotational Form

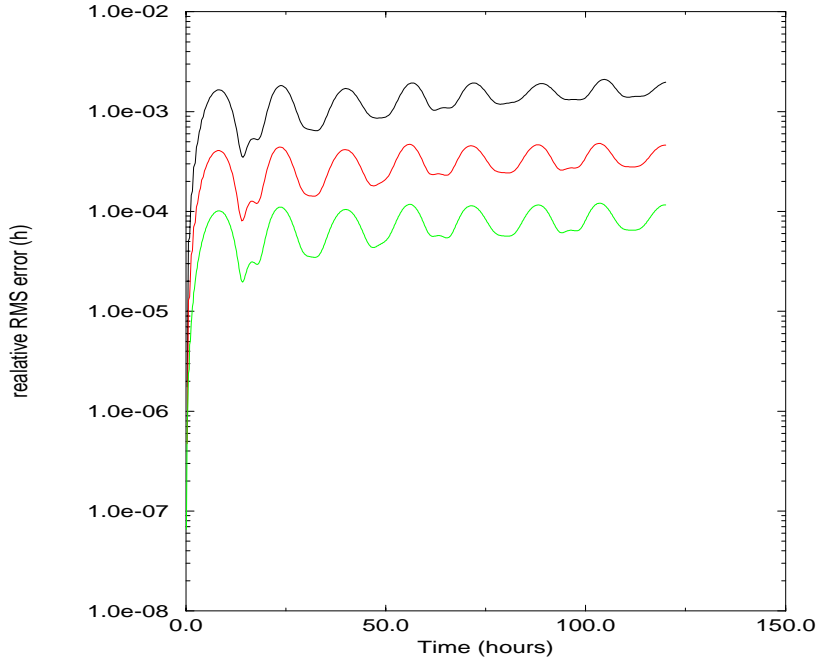


Fig. 6: Relative RMS Error in Height, Test Case 2, $q = 2, 3, 4$. Rotational Form

| Grid q | $l_\infty(\phi)$ | $l_2(\phi)$ | $l_\infty(V)$ | $l_2(V)$ |
|----------|------------------|-------------|---------------|-----------|
| 2 | 1.563E-04 | 1.707E-04 | 1.462E-03 | 9.357E-04 |
| 3 | 1.007E-05 | 1.102E-05 | 9.744E-05 | 6.352E-05 |
| 4 | 5.414E-05 | 5.671E-06 | 3.668E-05 | 5.486E-06 |

Table 2: Final Error in Case 2 for $q = 2, 3, 4$. $N=16$, $npts=13$

in Table 2.

The fourth order method on 16-19 points without diffusion for test case 2 gives errors as shown in Table 3.

4.2 ZONAL FLOW OVER AN ISOLATED MOUNTAIN

This test case is the only one with orography. A 5400m mountain is given through the surface height function, h_s . No analytical solution is known for this case so the usefulness of the case is in diagnosing the conservation properties of the numerical scheme. The simulation used

| Grid q | $l_\infty(\phi)$ | $l_2(\phi)$ | $l_\infty(V)$ | $l_2(V)$ |
|----------|------------------|-------------|---------------|-----------|
| 2 | 2.788E-04 | 3.025E-04 | 2.269E-03 | 1.550E-03 |
| 3 | 1.779E-05 | 1.947E-05 | 1.716E-04 | 1.120E-04 |
| 4 | 3.298E-06 | 1.806E-06 | 1.281E-05 | 7.614E-06 |

Table 3: Final Error in Case 2 for $q = 2, 3, 4$. $N=25$, $npts=19$

a diffusion coefficient of $eps_V = 5.0 \times 10^5$ with a timestep of 600 seconds for the $q = 4$ mesh.

The following normalized integral quantities are presented as a function of time: mass, total energy, potential enstrophy. The vorticity is presented as an integral without normalization in Figure 7. The conservation properties of the Cartesian method are much better than expected considering that the difference formula used to approximate the conservation of mass are not in flux form and are not guaranteed to preserve the global mass. The excellent conservation of enstrophy and vorticity are also a surprise. As normalized integrals it is not evident from Figure 7 that the integral of enstrophy maintains a value near machine zero ($\approx 10^{-13}$) throughout the simulation.

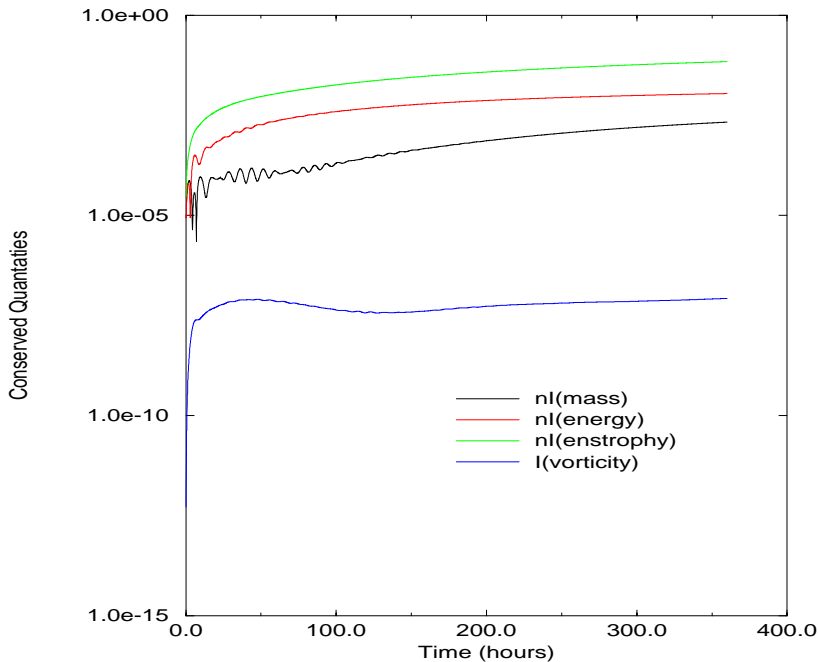
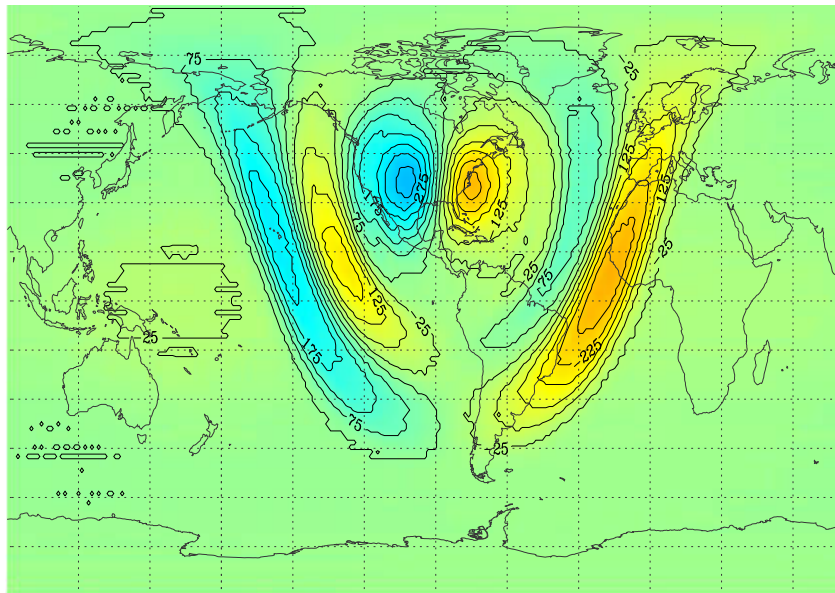


Fig. 7: Conserved integral quantities. Test Case 5, $q = 4$. Rotational Form

A contour plot a wave generated by the intrusion of the orographic forcing on the initial conditions is given in Figure 8. The plot shows the geopotential minus the initial condition so that the wave is clearly visible. At 18 hours the wave has reached the antipole of the mountain in the southern hemisphere. Figure 9 shows the development of the geopotential structure around the mountain as well as the confluence of the waves at the antipole. These cases used a 6th order method ($npts = 43$ and $N = 49$) with momentum diffusion of $\epsilon_V = 5 \times 10^5$. The grid used is the uniform icosahedral $q = 5$. The next experiment used a focused icosahedral grid with a second order discretization compared with a uniform grid and a fifth order discretization. Results are for day 15 of the integration. The low order focused ($q = 4$)-grid result Figure 10 compares favorably with the high order uniform ($q = 5$)-grid result Figure 11. Shown are the

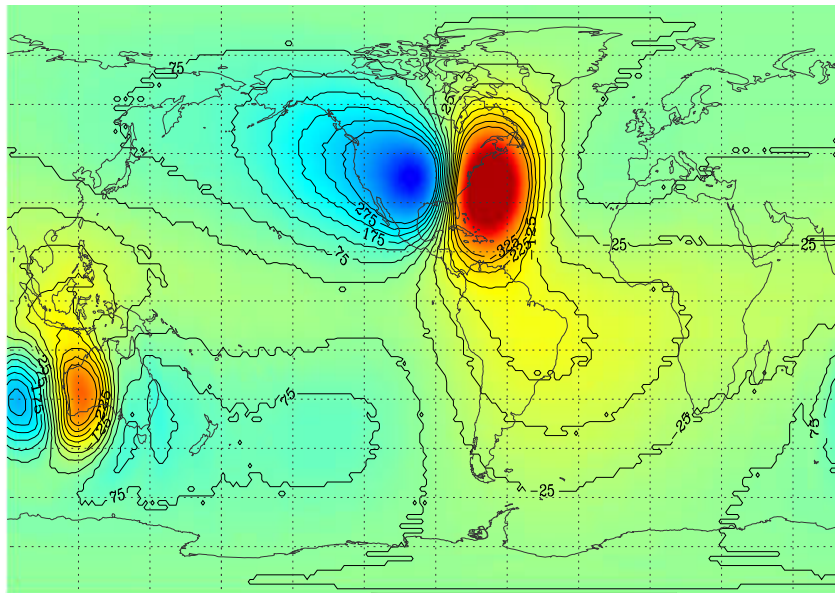
Case 5 phi at time 6. hrs
65_6_1 minus Initial Condition



Contour From -325 to 325 by 50.0 meters

Fig. 8: Initial condition wave, Test Case 5, 6th order at 6 hrs

Case 5 phi at time 18. hrs
65_6_1 minus Initial Condition



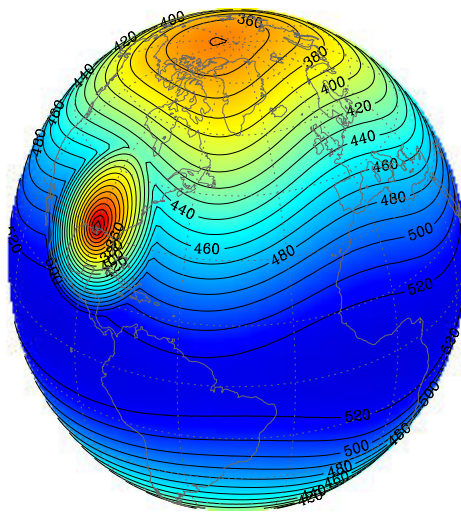
Contour From -325 to 325 by 50.0 meters

Fig. 9: Initial wave, Test Case 5, 6th order at 18 hrs

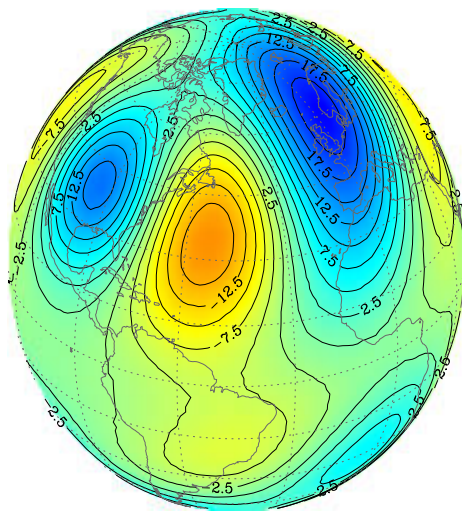
Case 5 phi at time 360. hrs

33x_2_1b Solution

33x_2_1b minus Initial Condition



Contour From 290 to 530 by 10.0 x 100 meters



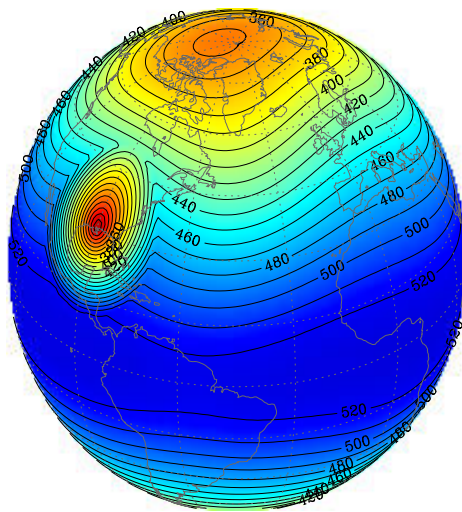
Contour From -35 to 35 by 2.5 x 100 meters

Fig. 10: Focused grid, 2nd order at 15 days

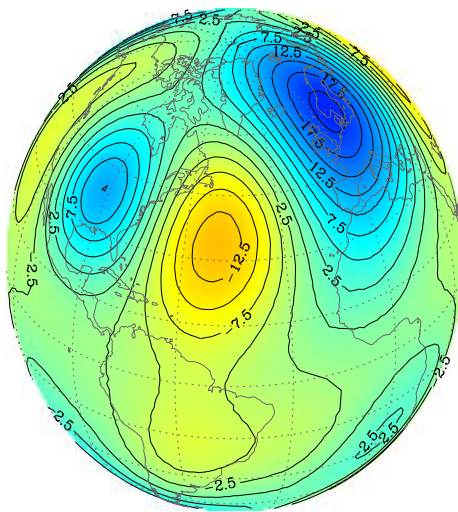
Case 5 phi at time 360. hrs

65_5_1 Solution

65_5_1 minus Initial Condition



Contour From 290 to 530 by 10.0 x 100 meters



Contour From -35 to 35 by 2.5 x 100 meters

Fig. 11: Uniform grid, 5th order at 15 days

geopotential (less the surface geopotential) and the same field minus the initial condition. The mature development of the lee wave is shown. The focused grid solution has a deeper trough in front of the mountain than exhibited by the uniform grid solution. The difference plots also show a greater definition of the wave structure in the focused grid solution.

4.3 ANALYZED 500mb INITIAL CONDITIONS

The real data initial conditions differ in smoothness from the previous cases exhibiting much finer scale structure and sharper gradients. For non-linear calculations there will be stronger interaction of modes and more active dispersive phenomena.

The first test case using analyzed atmospheric conditions is for 000GMT 21 December 1978. The spectral non-linear normal mode analysis has been used to filter gravity waves from this data. The NCAR netCDF file “REF0077.cdf” was used for initial conditions of both geopotential and velocity at the icosahedral grid points. The strong flow over the north pole has been useful in diagnosing pole problems for several numerical schemes.

Figure 12 shows the conserved quantities of mass, energy, enstrophy as normalized integrals and the conserved integral of vorticity through the simulation.

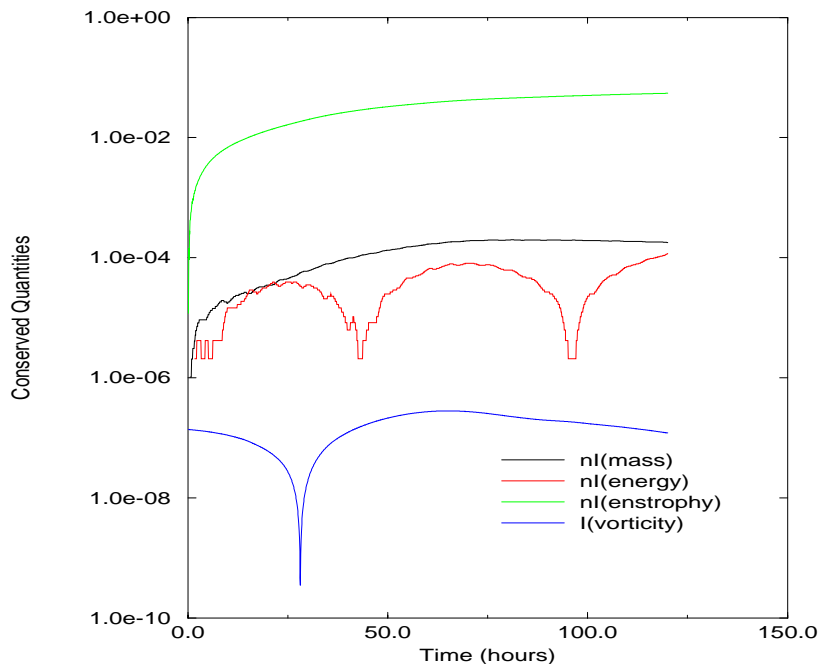
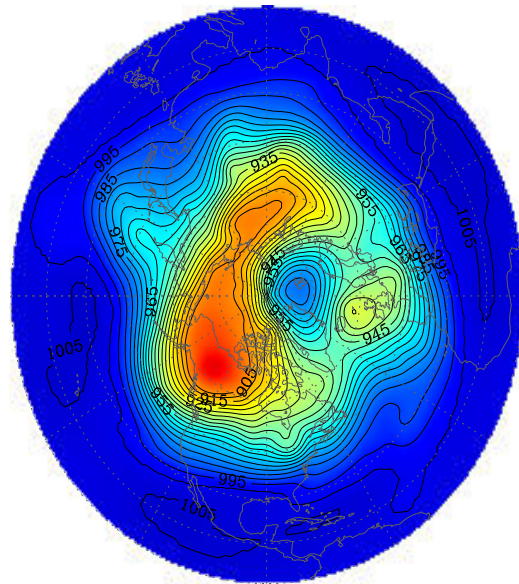


Fig. 12: Conserved integral quantities. Test Case 7a, $q = 5$.

Figure 13 shows the reference solution at 5 days generated by the NCAR spectral transform shallow water model [12].

Case 7a phi at time 120. hrs
Reference Solution



Contour From 900 to 1025 by 5 x100 meters

Fig. 13: Reference Solution at 5 Days

The high order Cartesian method solution is compared with the reference solution in Figure 14. The Cartesian solution was unable to isolate the small low at the zeroth meridian. The

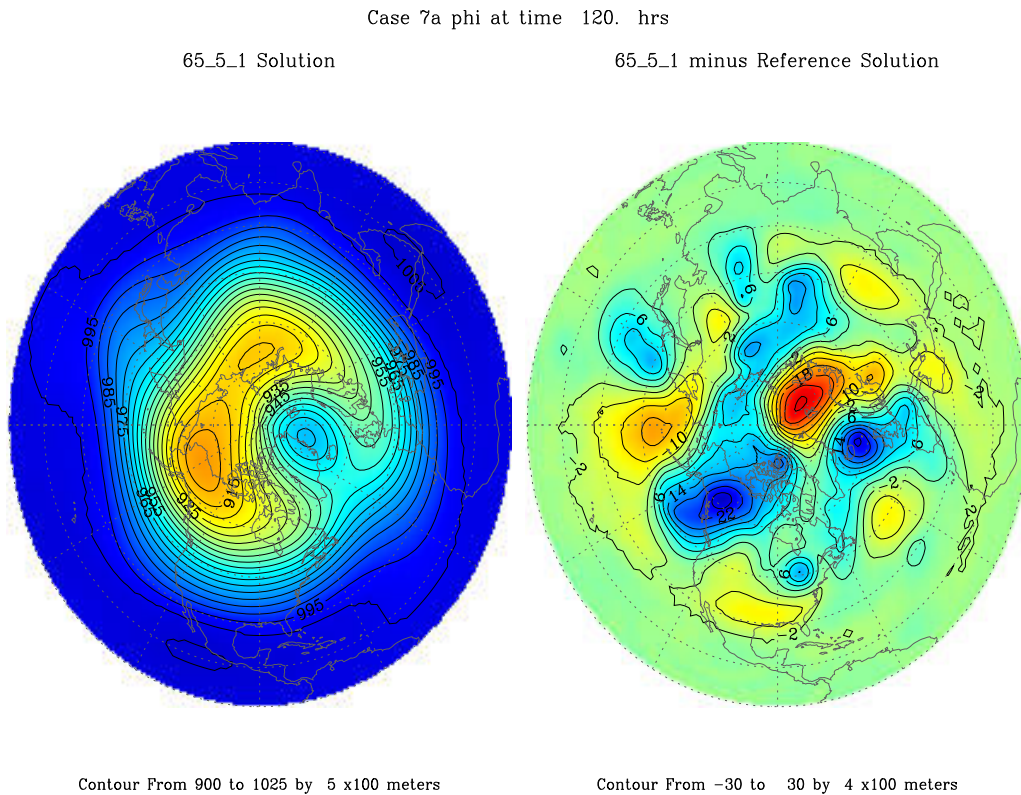


Fig. 14: Cartesian Solution at day 5, Fifth order, uniform ($q = 5$)-grid

method is overly diffusive and the solution has smoothed much of the relevant detail.

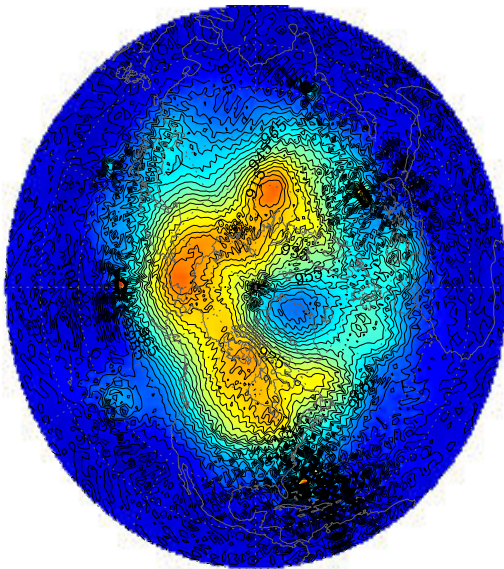
Stability of the high order methods for this test case was problematic. A smooth approximation for the derivatives, based on an underdetermined least squares produced the best results. For the fifth order method, a we choose $npts = 43$ and $N = 35$. The failure modes of the overdetermined approximations exhibited an error growth around the icosahedral grids base points. Figure 15 shows an unstable solution of a second order ($N = 9$, $npts = 7$) method using a focused grid after 2 days. Clearly visible are the (red) base points as the solution falls apart. This instability is controlled by using the underdetermined second order approximation ($N = 9$, $npts = 13$). Figure 16 shows the focused grid solution at 5 days. This is comparable to the uniform high order solution.

Another mode of instability on the focused grid arises from the selection of a diffusion

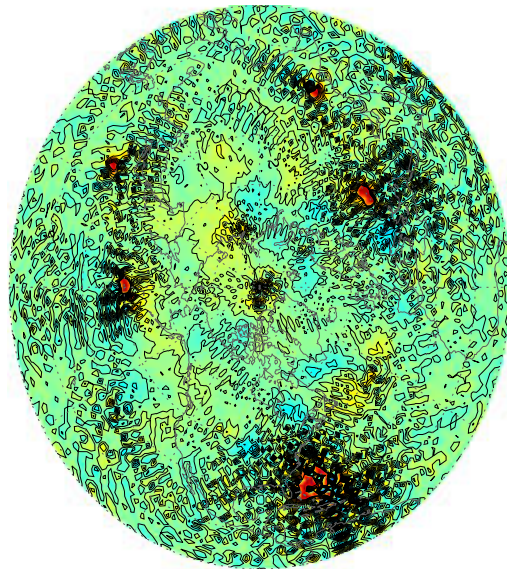
Case 7a phi at time 48. hrs

33x_2_1o Solution

33x_2_1o minus Reference Solution



Contour From 900 to 1025 by 5 x100 meters



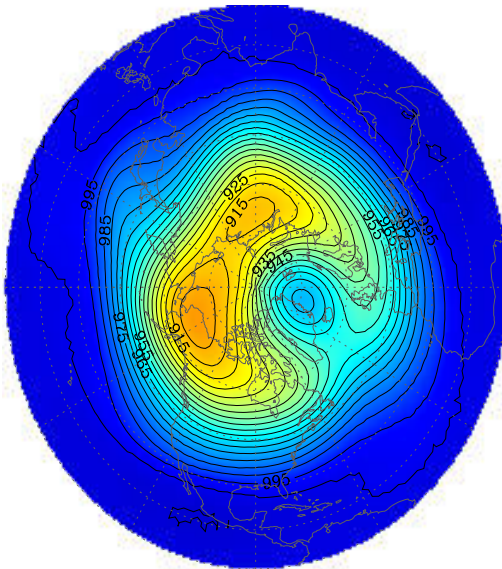
Contour From -30 to 30 by 4 x100 meters

Fig. 15: Instability of overdetermined, focused approximation, ($q = 4$)-grid

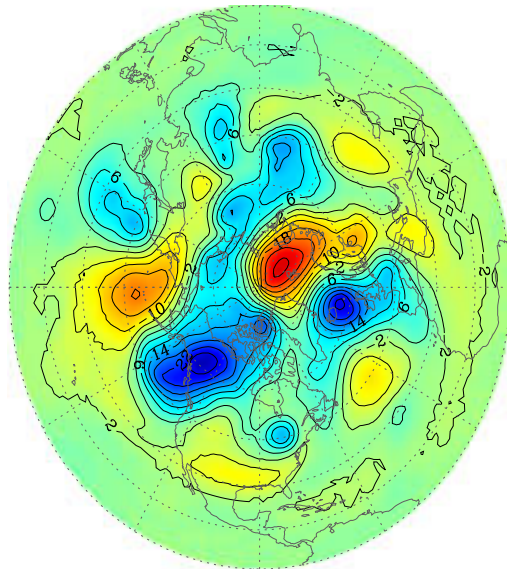
Case 7a phi at time 120. hrs

33x_2_1b Solution

33x_2_1b minus Reference Solution



Contour From 900 to 1025 by 5 x100 meters



Contour From -30 to 30 by 4 x100 meters

Fig. 16: Underdetermined, focused approximation, ($q = 4$)-grid

coefficient that is appropriate for the grid scales. Not enough diffusion (or too much) on the coarse portion of the grid will cause the solution to become unstable. Figure 17 shows the focused grid solution at 4 days for a fifth order (overdetermined) method. The error growth is occurring outside the high resolution area of the focused grid.

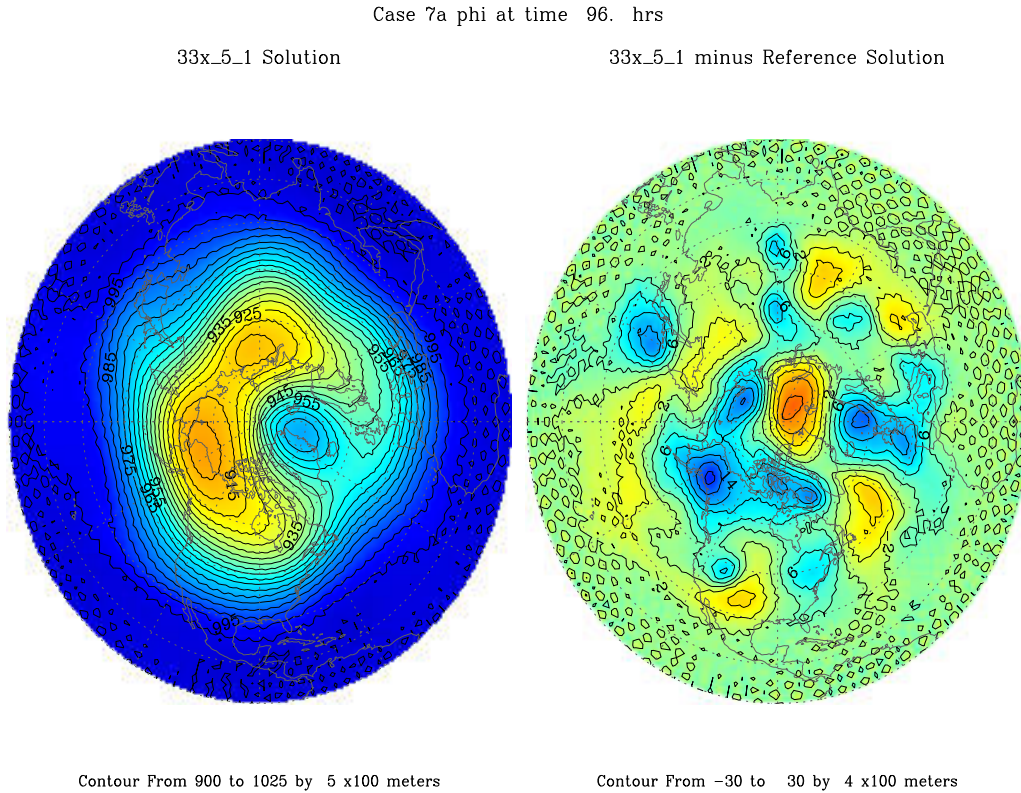


Fig. 17: Focused approximation, Fifth order, ($q = 4$)-grid

The error in the geopotential, measured globally, is compared as a function of time for several methods in Figure 18. The legend uses an “x” for the focused grids and the 33 or 65 refers to the $q = 4, 5$ grids. The order of the method is also indicated as either 2 or 5. What we observe is that the 5th order methods (solid lines) are generally more accurate globally than the second order methods. The focused grids appear to be worse in this measure, because the coarse resolution portion of the globe has a larger error. If the error measure is restricted to only northern hemisphere points, then the situation is reversed. Focused grid integrations are more accurate than their uniform grid counterparts. In fact, the focused ($q = 4$)-grid is as accurate as the uniform ($q = 5$)-grid.

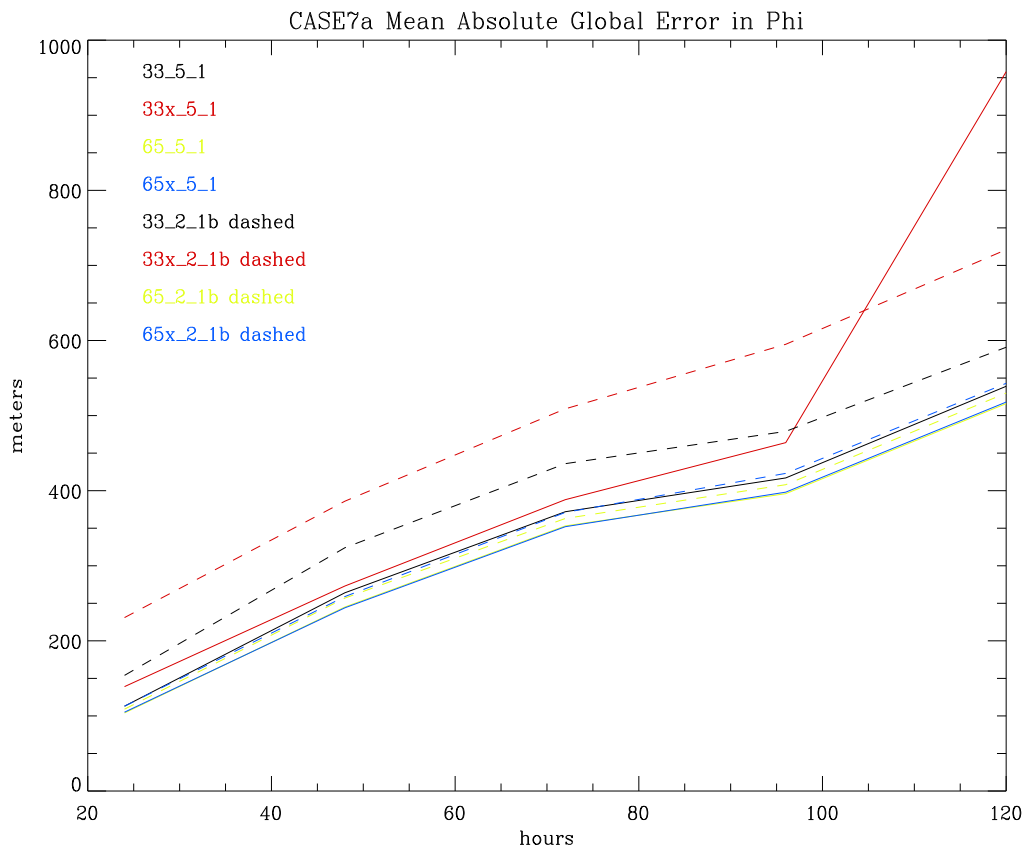


Fig. 18: Global Mean Absolute Error Comparison

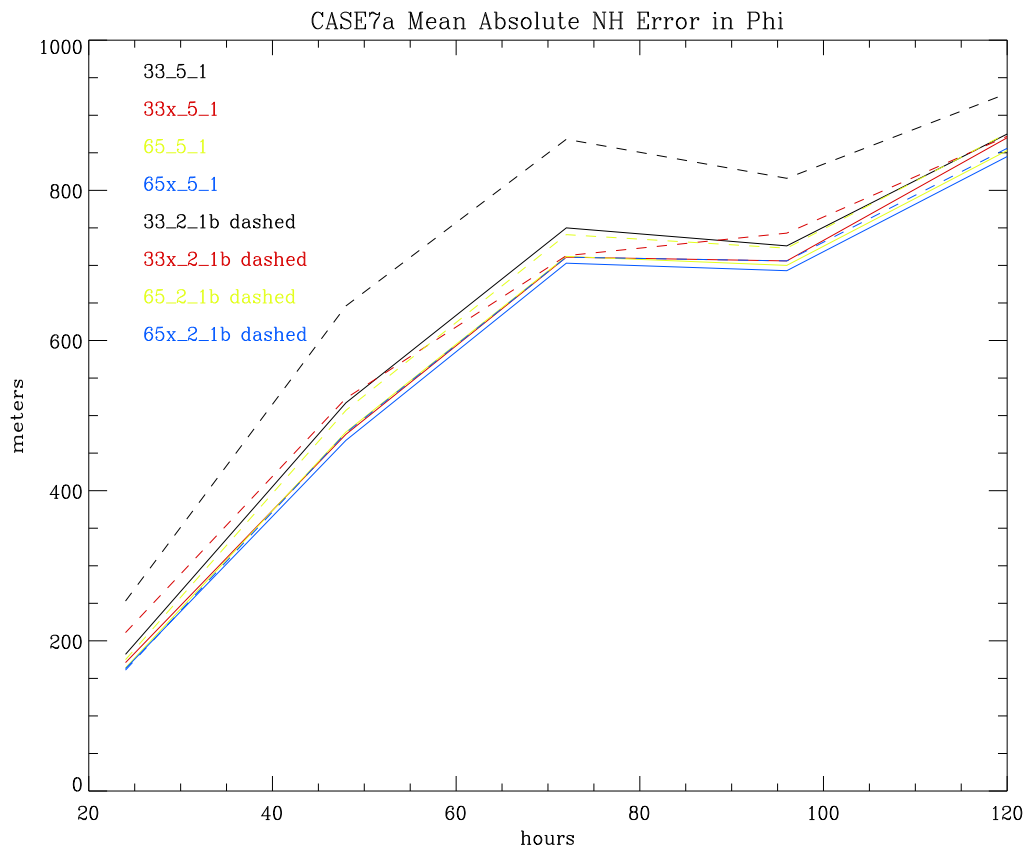


Fig. 19: Northern Hemisphere Mean Absolute Error Comparison

5 CONCLUSIONS

Numerical methods for the shallow water equations on the sphere are faced with three hurdles. First, the accuracy of the geostrophic wind balance. The numerical approximation for the gradient of the geopotential must balance the Coriolis term well. Since the Coriolis term does not involve derivatives the gradient approximation is crucial to achieve a reasonable balance. Second, the pole problem. Since the spherical coordinate representation of the velocity is singular at the poles, derivatives must be approximated with care. The third hurdle is stability.

In our work, the first hurdle has been passed by adopting a co-located velocity and gradient approximation. The collocation method with accurate approximations for the derivatives gives an excellent balance of the geostrophic wind terms. The Cartesian method is free of the pole problem since velocities are continuous at the poles. The higher order approximations must be stabilized for long integrations. First, artificial diffusion was added by the inclusion of a Laplacian term to the momentum equation. Second, an implicit method was adopted which has shown some promise for symmetric time integrations. Finally, the smoothness of the derivative approximations was adjusted.

Stable integrations of two of the shallow water test cases were described for a variety of approximation orders and icosahedral grids. We concluded that the high order methods are overly diffusive when stabilized for long integrations. Other stabilization techniques are required to realize the benefits of the high order approximations.

References

- [1] I-Liang Chern. A Control Volume Method on a Icosahedral Grid for Numerical Integration of the Shallow-water Equations on the Sphere . MCS preprint, Argonne National Laboratory, Chicago, IL, 1991.
- [2] J. Cote, M. Roch, A. Staniforth, and L. Fillion. A variable-resolution semi-lagrangian finite-element global model of the shallow water equations. *Mon. Wea. Rev.*, 121:231–243, 1993.
- [3] P. Courtier and J.-F. Geleyn. A global numerical weather prediction model with variable resolution: Application to the shallow-water equations. *Quart. J. Roy. Met. Soc.*, 114:1321–1346, 1988.
- [4] M.S. Fox-Rabinovitz, G.L. Stenchikov, M.J. Suarez, and L.L. Takacs. A finite-difference GCM dynamical core with a variable-resolution stretched grid. *Mon. Wea. Rev.*, 125:2943–2968, 1997.
- [5] E. Hairer and C. Lubich. Asymptotic expansions and backward analysis for numerical integrators. *unknown*, 1998.
- [6] E. Hairer and D. Stoffer. Reversible long-term integration with variable stepsizes. *SIAM J. Sci. Comput.*, 18:257–269, 1997.
- [7] Ross Heikes and David A. Randall. Numerical Integration of the Shallow-Water Equations on a Twisted Icosahedral Grid. Part I. *Mon. Wea. Rev.*, 123:1862–1880, 1995.
- [8] Ross Heikes and David A. Randall. Numerical Integration of the Shallow-Water Equations on a Twisted Icosahedral Grid. Part II. *Mon. Wea. Rev.*, 123:1881–1887, 1995.
- [9] C.L. Lawson and R.J. Hanson. *Solving Least Squares Problems*. Prentice-Hall, Englewood Cliffs, NJ, 1974.
- [10] B. Machenhauer. The spectral method. In *Numerical Methods Used in Atmospheric Models*, volume II of *GARP Pub. Ser. No. 17. JOC*, chapter 3, pages 121–275. World Meteorological Organization, Geneva, Switzerland, 1979.
- [11] Y. Masuda and H. Ohnishi. An Integration Scheme of the Primitive Equation Model with an Icosahedral-Hexagonal Grid System and its Application to the Shallow Water Equations. In *Short- and Medium-Range Numerical Weather Prediction*, pages 317–326, 1986.

- [12] J.J. Hack R. Jakob and D.L. Williamson. Reference solutions to shallow water test set using the spectral transform method. Near tech note, National Center for Atmospheric Research, Boulder, CO, 1993.
- [13] R. Sadourny, A. Arakawa, and Y. Mintz. Integration of the Nondivergent Barotropic Vorticity Equation with an Icosahedral-Hexagonal Grid for the Sphere. *Mon. Wea. Rev.*, 96:351–356, 1968.
- [14] R. Sadourny and P. Morel. A Finite-Difference Approximation of the Primitive Equations for a Hexagonal Grid on a Plane. *Mon. Wea. Rev.*, 97:439–445, 1969.
- [15] J.M. Sanz-Serna. Studies in numerical nonlinear instability i. why do leapfrog schemes go unstable? *SIAM J. Sci. Statist. Comput.*, 6:923–938, 1985.
- [16] Frank Schmidt. Variable fine mesh in spectral global models. *Beitrage zur Physik der Atm.*, 50:211–217, 1977.
- [17] I. A. Stegun. Legendre functions. In M. Abramowitz and I. A. Stegun, editors, *Handbook of Mathematical Functions*, chapter 8, pages 332–353. Dover Publications, New York, 1972.
- [18] P. N. Swarztrauber. The Approximation of Vector Functions and Their Derivatives on the Sphere. *SIAM J. Numer. Anal.*, 18:191–210, 1981.
- [19] P.N. Swarztrauber. Spectral Transform Methods for Solving the Shallow-Water Equations on the Sphere. *Mon. Wea. Rev.*, 124(4):730–744, 1996.
- [20] P.N. Swarztrauber, D.L. Williamson, and J.B. Drake. The Cartesian Method for Solving of PDE's in Spherical Geometry. *Dyn. Atm. Ocn.*, 27:679–706, 1997.
- [21] A.N. Tikhonov and A.A. Samarskii. *Equations of Mathematical Physics*. Dover Publications, New York, 1963.
- [22] D. L. Williamson. Integration of the Barotropic Vorticity Equation on a Spherical Geodesic Grid. *Tellus*, 20:642–653, 1968.
- [23] D. L. Williamson. Integration of the Primitive Barotropic Model Over a Spherical Geodesic Grid. *Mon. Wea. Rev.*, 98:512–520, 1969.
- [24] D. L. Williamson. Numerical Integration of Fluid Flow Over Triangular Grids. *Mon. Wea. Rev.*, 97:885–895, 1969.

- [25] D. L. Williamson. A Comparison of First- and Second-Order Difference Approximations over a Spherical Geodesic Grid. *J. Comp. Phys.*, 7:301–309, 1971.
- [26] D. L. Williamson. *Numerical Methods Used in Atmospheric Models*, chapter 2, pages 51–120. GARP Pub. Ser. No. 17. JOC, WMO, Geneva, Switzerland, 1979.
- [27] D. L. Williamson, J.B. Drake, J.J. Hack, Rudiger Jakob, and P.N. Swarztrauber. A Standard Test Set for Numerical Approximations to the Shallow Water Equations on the Sphere. *J. Comp. Phys.*, pages 211–224, 1992.
- [28] K. Yessad and P. Benard. Introduction of a local mapping factor in the spectral part of the meteo-france global variable mesh numerical forecast model. *Quart. J. Roy. Met. Soc.*, 122:1701–1719, 1996.

INTERNAL DISTRIBUTION

- 1-5. J. B. Drake
- 6. Central Research Library
- 7. ORNL Laboratory Records RC
- 8-20. ORNL Laboratory Records OSTI

EXTERNAL DISTRIBUTION

- 21. Daniel X. Guo, Department of Mathematics and Statistics, University of North Carolina at Wilmington, Wilmington, NC 94550